Double-handed circular Bragg phenomena in polygonal helix thin films

Andy C. van Popta,[a] Michael J. Brett, and Jeremy C. Sit
Department of Electrical and Computer Engineering, University of Alberta, Edmonton, Alberta, T6G 2V4, Canada

(Received 5 July 2005; accepted 15 September 2005; published online 24 October 2005)

Oblique-incidence physical vapor deposition has been used to create optical thin films with a polygonal helix-shaped nanostructure. A series of titanium dioxide thin films are investigated, including triangle, square, pentagon, and star-shaped polygonal helices. Experimental optical measurements reveal a double-handed circular Bragg response: at one frequency band a polygonal helix reflects left-handed circularly polarized light, and at a second frequency band reflects right-handed circularly polarized light. The relative wavelength dependence of each reflection band is determined by the physical structure of the polygonal helix, a property that is set during the thin-film deposition process. Spectral-hole polarization filters, produced by adding twist and spacing layer defects to polygonal helix thin films, are also reported. © *2005 American Institute of Physics*. [DOI: 10.1063/1.2115092]

I. INTRODUCTION

Many materials, both self-assembling and artificially constructed, are being studied for their photonic properties at optical frequencies. When a dielectric material has an ordered physical structure with a spatial periodicity that is comparable to optical wavelengths, it will act as a photonic band-gap crystal.[1,2] Wavelengths of light that fall within the band gap cannot propagate through the photonic crystal; instead the light is reflected. Often the most technically difficult types of photonic crystals to fabricate are three-dimensional (3D) photonic crystals, especially when intentional defects such as waveguides and cavities are required.[3,4] Fabrication is simplified when the photonic crystal has structural ordering in fewer spatial dimensions. In particular, there are materials that act as one-dimensional (1D) photonic crystals for circularly polarized light and exhibit a pseudo-band-gap at optical wavelengths. Within the band gap, these chiral filters reflect circularly polarized light of one handedness while allowing circularly polarized light of the opposite handedness to freely propagate.

Both organic and inorganic chiral filters are being studied for reflective displays,[5,6] laser mirrors,[7] and sensors.[8] Organic chiral filters include cholesteric liquid crystals (CLCs), which consist of rodlike molecules that arrange themselves into a helical structure.[9] CLCs can be divided into parallel nematic sheets that are perpendicular to the helical axis. Within each sheet a local director indicates the preferred average orientation of the rodlike molecules. From sheet to sheet, the director twists slightly to trace out either a left-handed or a right-handed helical structure. Circularly polarized light of the same handedness is reflected by the CLCs in a band of wavelengths that is proportional to the helical pitch.

Inorganic chiral filters can be formed by modern thin-film deposition techniques, including glancing angle deposition[10,11] (GLAD) and serial bideposition (SBD).[12] Both techniques utilize physical vapor deposition (PVD) at highly oblique vapor incidence angles to create columnar thin films. By adding substrate rotation, the columnar morphology can be shaped into helical structures that exhibit the same circular Bragg effects that are witnessed in CLCs. The advantage of using PVD is the ability to easily modify the helical structure and composition of a chiral filter, modifications that are very difficult or impossible to accomplish in CLCs.

In this study, we examine how GLAD can be used to fabricate polygonal helices. In traditional chiral filters, circular Bragg reflections are caused by a continuous and gradual rotation of a local linear birefringence throughout the thickness of the filter. A polygonal helix, on the other hand, is formed by discrete layers where the local birefringence makes abrupt rotations between layers and remains fixed within each layer. These abrupt rotations can create a double-handed optical response. At one frequency band, a polygonal helix will reflect left-handed circularly polarized light (LCP) and at a second frequency band reflects right-handed circularly polarized light (RCP). The relative position of each reflection band is related to the rotation angle between subsequent layers of the polygonal helix (i.e., the number of sides of the polygonal helix). We report here on the experimental fabrication and characterization of triangle, square, star, and pentagon-type polygonal helices.

Serial bideposition has been used to study ambichiral structures, which are very similar to polygonal helices. SBD uses rapid 180° substrate rotations to produce biaxial plates where the principal indices of refraction are parallel and perpendicular to the substrate. If the orientation of the biaxial plates is rotated about the substrate normal in discrete intervals, an ambichiral filter can be formed. Simulations have been used to study the optical properties of ambichiral films and experimental measurements have been made for the case where the biaxial plates are rotated in 45° increments.[13,14] The advantage of using SBD is that it enhances the local linear birefringence in the plane of the substrate, which in turn strengthens circular Bragg reflectance. However, the

[a]Electronic mail: vanpopta@ualberta.ca

deposition rate must be kept relatively low (0.15 nm/s) to limit film deposition during substrate rotation (which will tend to reduce the local birefringence). Additionally, the birefringence of SBD films is strongly dependent on the arm thickness that is deposited between 180° substrate rotations.[12] This makes it more difficult to reproduce films that are formed by SBD because the optical anisotropies are sensitive to the large deposition rate fluctuations that can occur during PVD processing. GLAD can be used to deposit reproducible chiral filters at much higher deposition rates. The circular Bragg effects in GLAD films are also enhanced by the structural handedness of the helix, an effect that will be discussed in Sec. V. In this study, we use polygonal helices to confirm the basic optical phenomena observed in ambichiral films, and present results on the incorporation of defect modes in polygonal helices.

Adding an intentional imperfection to the periodic structure of a photonic crystal can create a defect mode within the larger band gap of the crystal. In a chiral filter the simplest way to introduce a defect mode is to incorporate a phase discontinuity to the circular Bragg grating by adding either an isotropic spacing layer or a twist defect to the helical structure. The defect mode appears as a narrow bandpass, or spectral hole, within the larger circular reflection band of the chiral filter.[15,16] Defect modes are very useful for a number of devices, including humidity sensors,[8] low threshold lasers,[17,18] and microwaveguides.[19] Twist defects have been successfully added to CLCs by careful alignment of two highly polymerized films.[20,21] However, variations in the helical pitch, layer adhesion, and alignment angle can cause the defect mode to become averaged out over sufficiently large areas.[20] PVD fabrication of inorganic chiral filters permits the incorporation of defects with relative ease. We report on the use of both twist defects and spacing layer defects in polygonal helix thin films.

II. THEORY

Physical vapor deposition will produce thin films with a columnar microstructure for substrate temperatures that are low relative to the vapor melting point. If the substrate is then tilted at an oblique angle to the impinging vapor molecules, topographical variations due to adatom clustering and nucleation will shadow regions of the substrate. Nucleation sites will evolve into columns that tilt towards the incoming vapor stream, which creates self-shadowing growth. Because there is no shadowing perpendicular to the deposition plane, columns can fan out laterally and chain together, creating a second structural anisotropy.[22] Fanning of columns creates linear form birefringence in the plane of the substrate and is responsible for the film's biaxial properties.

GLAD combines highly oblique deposition with computer-controlled substrate motion to shape the inclined columns into more complex film architectures. For instance, abrupt 180° turns of the substrate will generate a zigzag film structure, while rapid substrate rotation will result in a GLAD film composed of vertical posts. A regular helix is deposited by slow, continuous substrate rotation. The pitch of the helix is determined by the rotation speed, relative to the deposition rate, and the helical handedness is set by the direction of substrate rotation. All of the films used in this study were deposited with a right-handed helical structure by making clockwise rotations of the substrate as seen looking towards the sample from the perspective of the evaporation source. The pitch of each helix was chosen to place the circular reflection bands within the visible to near-infrared wavelength regime.

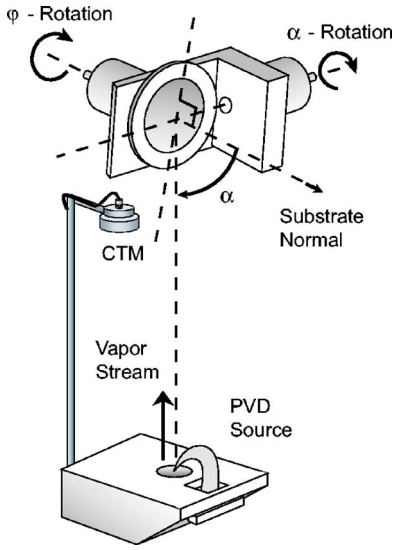

FIG. 1. Schematic of the GLAD apparatus.

A schematic of the GLAD setup is shown in Fig. 1.[23] The α motor controls the deposition angle and the φ motor controls the azimuthal angle of the substrate. Using this deposition setup, the user can control the film's nanostructure, porosity, and chemical composition. GLAD has been successfully applied to semiconductors, dielectrics, and metals using thermal and electron-beam evaporation, long-throw low-pressure sputtering,[24] and pulsed laser deposition.[25] The versatility of the GLAD process has lead to its application in a variety of fields including field emitters,[26] supercapacitors,[27] carbon electrodes,[28] antireflection coatings,[29] thermal barrier coatings,[30] and solar cells,[31] to name a few.

In contrast to the continuous substrate rotation used to fabricate a regular helix, a polygonal helix is formed by abrupt $2\pi/m$ rotations each time the film thickness has increased by p/m, where p is the pitch of the helix and m is the number of sides of polygonal helix. For example, $m=3$ for a triangle helix and $m=4$ for a square helix (note, however, that m need not be a whole number). Figure 2 is an illustration that compares the basic structure of a regular or circular helix to a polygonal helix. At highly oblique deposition angles ($\alpha>70°$) the substrate rotations used to produce a polygonal helix must be slowed down to prevent significant broadening between arms of the helix. However, all of the films used in this study were deposited at $\alpha=65°$, resulting in denser films and eliminating the need to apply the slow corner growth technique.[32]

The chosen deposition angle of 65° also produces the strongest circular Bragg reflections.[33] If the deposition angle is reduced the film's optical anisotropies will diminish and

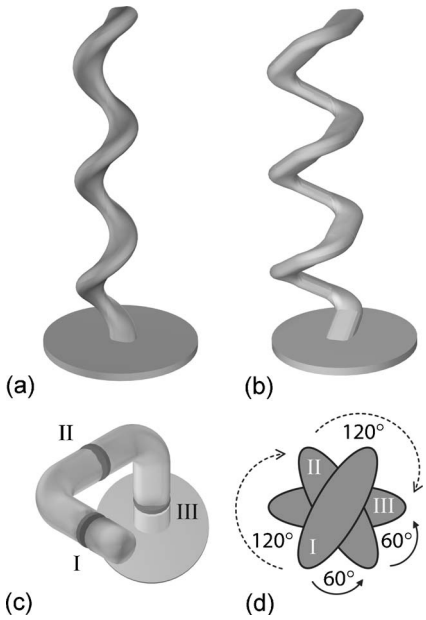

FIG. 2. (a) A circular helix, (b) a triangle helix, and (c) the top-view of a single-turn triangle helix. (d) A triangle helix can be described as a stack of biaxial plates that rotate by 120° increments in the clockwise direction as seen by RCP light and by 60° increments in the counterclockwise direction as seen by LCP light.

become completely isotropic as α tends to zero. Conversely, if the deposition angle is increased, substrate shadowing is enhanced and the film becomes much more porous. According to effective-medium theory, a medium that is composed of a mixture of materials exhibits an effective refractive index that depends on the relative amounts of the constituents and the size of the inclusions.[34] A GLAD film is essentially a mixture of solid film material and air-filled pores; as the pores grow in number and size, the effective index of the film decreases, resulting in a lower form birefringence despite the enhanced structural anisotropies.[35] Diffuse scattering is also increased at highly oblique deposition angles due to the proliferation of air/film interfaces, which causes the filter to have a hazy appearance. Furthermore, at $\alpha > 70°$ the helical film morphology transforms from close-packed columns into individual helical structures. The growth of these isolated helical columns is inherently unstable. Topographical variations cause certain helical columns to become extinct while others broaden to maintain a constant film density, which is fixed by the deposition angle. When helical columns broaden they lose definition and no longer strengthen the film's circular Bragg reflectance beyond a critical thickness.[36]

Aside from higher-order harmonics, a regular helical thin film contains a single circular reflection band centered at the Bragg wavelength

$$\lambda_o^{\mathrm{Br}} = n_{\mathrm{avg}} p, \tag{1}$$

where n_{avg} is the average refractive index. The film will reflect RCP light when the helix structure is right-handed and LCP light when the helix structure is left-handed. A polygonal helix, on the other hand, contains two reflection bands, a primary circular reflection band at λ_o^{Br} and an inverted reflection band centered at

$$\lambda_o^{\mathrm{inv}} = 2(m-2)^{-1} n_{\mathrm{avg}} p = \xi(\pi - \xi)^{-1} n_{\mathrm{avg}} p, \tag{2}$$

where ξ is the angular rotation of the substrate between each arm of the polygonal helix (in radians). At λ_o^{inv}, a polygonal helix will reflect circularly polarized light of the opposite handedness; a right-handed polygonal helix will reflect LCP light and a left-handed helix will reflect RCP light. To help understand this effect, Fig. 2(d) depicts a polygonal helix as a stack of birefringent plates. For a structurally right-handed polygonal helix, the birefringent plates rotate by ξ in the clockwise direction as "seen" by RCP light. LCP light also sees a rotation of the birefringent plates, but in the counterclockwise direction where each plate is rotated by $(\pi - \xi)$. The different rotation rates are responsible for the formation of two distinct reflection bands. For CLCs and circular helix films m is very large, placing the inverted reflection band at an arbitrarily high frequency, meaning that only the primary reflection band is measurable.

III. SAMPLE PREPARATION

All of the films used in this study were deposited by electron-beam evaporation onto unheated silicon wafers and glass substrates (Corning 7059). The evaporation source was rutile titanium dioxide (Cerac Inc., 99.9% pure), which was deposited in an $O_2(g)$ background pressure of 7×10^{-3} Pa, as measured by a calibrated ionization gauge located near the inlet of the vacuum chamber's diffusion pump. A 6 MHz crystal oscillator (CTM) was used to monitor the normal incidence deposition rate, which was typically 1.0–1.5 nm/s. After deposition, films were left in atmospheric conditions for at least 24 h before being characterized to facilitate residual oxidation.[37] Scanning electron microscopy (SEM) was used to examine film morphology and make measurements of the helical pitch and film thickness. Previous x-ray-diffraction measurements of TiO_2 films deposited under similar conditions have shown that the films are amorphous unless annealed.[38] All of the samples underwent optical characterization in a Class 100 clean room at the University of Alberta's Nanofabrication and Micromachining Facility, where the ambient humidity is maintained at $40\% \pm 5\%$ relative humidity (RH). The porous nature of a GLAD film does render the chiral filters sensitive to ambient humidity conditions. Water can condense in the pores of a GLAD film and alter the effective refractive index. However, the optical measurements were carried out at a stable humidity and any fluctuations are not expected to significantly have an impact to the characteristics under consideration in these experiments. In the future, GLAD films can be rendered insensitive to humidity by attaching self-assembled hydrophobic organic molecules to the internal surfaces of the film.[39]

IV. OPTICAL CHARACTERIZATION

A variable angle spectroscopic ellipsometer (J. A. Woollam Company Inc., model V-VASE) was used to measure the transmittance and Mueller matrix of each sample. The 4×4 Mueller matrix operates on Stokes vectors to relate input polarization states to output polarization states for a particular angle of incidence and wavelength.[40] Mueller matrix el-

ements can be used to evaluate circular Bragg phenomena, including the selective remittance of circularly polarized light and the optical rotation of linearly polarized light. For instance, the transmittance of LCP light and RCP light is calculated using Eqs. (3) and (4), respectively, and optical rotatory dispersion (ORD) is calculated using Eq. (5).

$$T(\mathrm{LCP}) = m_{11}(\lambda) - m_{14}(\lambda), \tag{3}$$

$$T(\mathrm{RCP}) = m_{11}(\lambda) + m_{14}(\lambda), \tag{4}$$

$$\mathrm{ORD}(\lambda, \phi) = \frac{1}{2}\arctan\frac{S_2}{S_1} + \frac{\pi}{2}u(-S_1)\mathrm{sgn}(S_2) - \phi, \tag{5}$$

$$S_1(\lambda, \phi) = m_{21}(\lambda) + m_{22}(\lambda)\cos 2\phi + m_{23}(\lambda)\sin 2\phi, \tag{6}$$

$$S_2(\lambda, \phi) = m_{31}(\lambda) + m_{32}(\lambda)\cos 2\phi + m_{33}(\lambda)\sin 2\phi, \tag{7}$$

where m_{ij} is the Mueller matrix element of the ith row and jth column, ϕ is the azimuthal angle of the incident linear polarization state, the unit step function $u(x)=1$ for $x \geqslant 0$ and $u(x)=0$ for $x<0$, and $\mathrm{sgn}(x)=1$ for $x \geqslant 0$ and $\mathrm{sgn}(x)=-1$ for $x<0$.

V. EXPERIMENTAL RESULTS AND DISCUSSION

To evaluate the optical properties of polygonal helices, a circular TiO_2 GLAD helix was first deposited under equivalent conditions and characterized for comparison. The helix consisted of 15 full turns with a pitch of 325 nm, as measured by SEM analysis. The optical rotatory dispersion expressed by the helix is shown in Fig. 3(a), and the normal incidence transmittance of LCP light and RCP light is shown in Fig. 3(b). The circular reflectance band is clearly shown by the anomalous optical rotation and drop in transmittance of RCP light at 626 nm. The maximum selective transmittance is 74% as shown in the inset of Fig. 3(b).

A set of polygonal helices, consisting of an 18-turn triangle helix, a 7-turn square helix, a 10-turn pentagon helix, and a 14-turn star helix, was deposited. Figure 4 is a SEM micrograph of the triangle helix. Close inspection of the film structure reveals the three distinct layers used to make up each turn of the triangle helix.

A star helix is formed when the angular rotation between each arm of the helix does not divide evenly into 360°. In this case, each arm of the star helix was grown by rotating the substrate through 105° [$m=24/7$ using Eq. (2)]. This creates a star-shaped pattern of biaxial plates which only repeats itself after 24 arm segments ($105° \times 24 = 14\pi$). The 14 turns of the star helix refer to the number of net 360° revolutions made by the φ motor during film deposition. The circular Bragg phenomena expressed by the star helix, as well as the other polygonal helices, are shown in Fig. 5.

Figure 5 demonstrates how the inverted reflection band can be shifted to shorter wavelengths, relative to the primary reflection band, by decreasing the angular rotation between arms of a polygonal helix. For a square helix the primary and inverted reflection bands overlap, leaving only a residual circular birefringence. When the angular rotation between arms is less than 90° the inverted reflection band moves from the low-frequency side to the high-frequency side of the primary reflection band [compare Fig. 5(a) to Fig. 5(d)]. To confirm Eq. (2), the λ_o^{inv} values taken from the films graphed in Fig. 5 are normalized by the wavelength of the primary reflection band and plotted versus the arm rotation angle ξ in Fig. 6. The small deviations between the calculated values and experimental results are caused by the dispersion of the average refractive index.

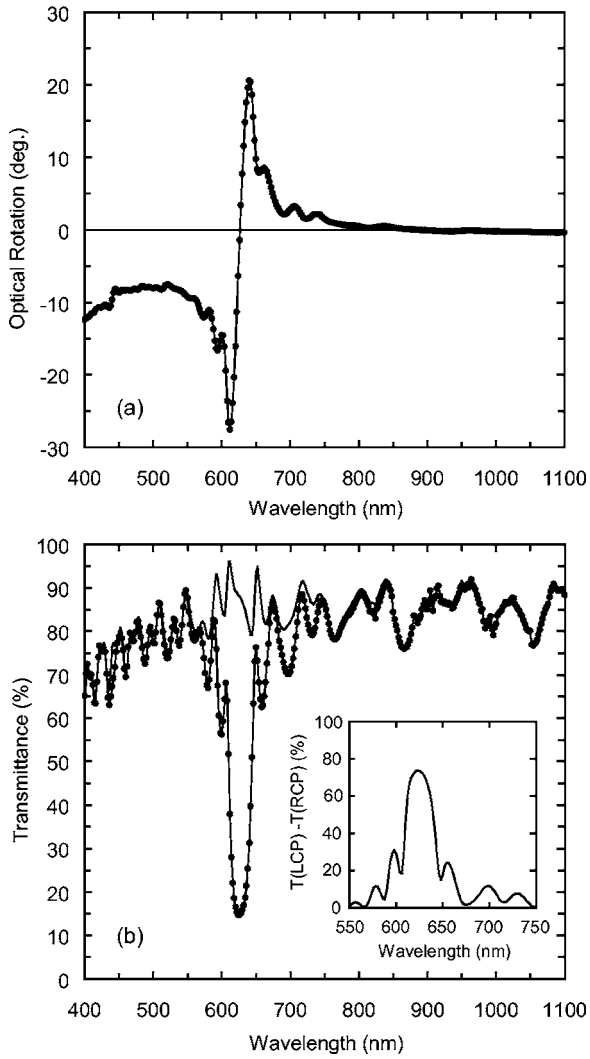

FIG. 3. Circular Bragg phenomena in a regular 15-turn TiO_2 helix: (a) optical rotatory dispersion and (b) transmittance of LCP light (solid line) and RCP light (dotted line). The inset plots the selective transmittance of circularly polarized light.

Stronger circular remittances can be achieved by adding more turns to a helix, increasing local linear birefringence, or by adding phase-matched antireflection coatings.[41] Figure 7 shows the increase in the maximum selective transmittance of circularly polarized light when additional turns are added to a triangle helix. The solid line was generated using a transfer-matrix simulation method,[42] where the polygonal helix is divided into parallel biaxial layers. The thickness of each layer is equal to the thickness of each arm of the helix, and the optical axis is rotated by $2\pi/m$ between subsequent layers. In this way, a thin-film stack resembling a chiral filter is created. For further details, the reader is encouraged to review the numerous publications on simulating thin-film

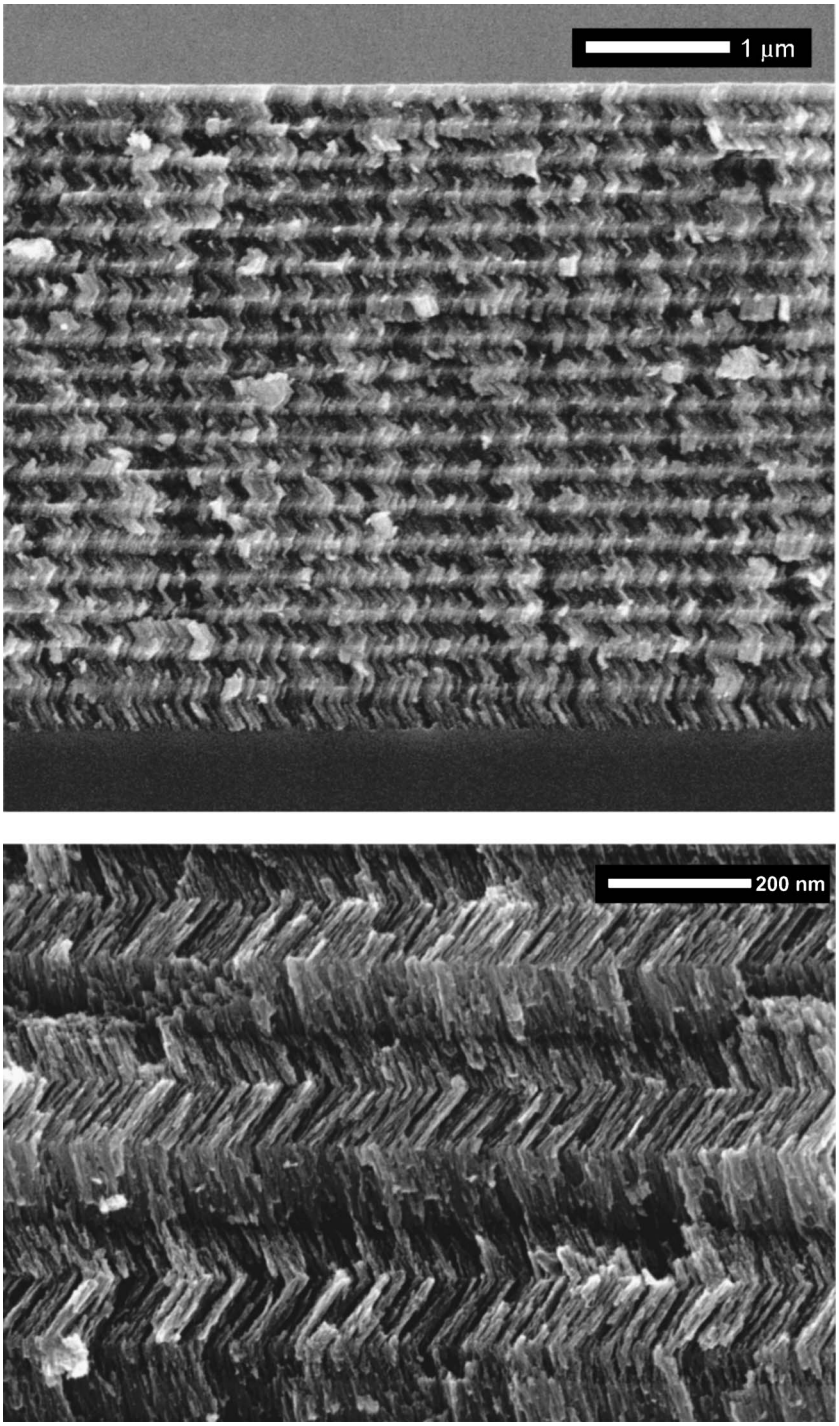

FIG. 4. SEM images of a triangle helix taken in a cross section.

helicoidal bianisotropic media.[43,44] The helical pitch, handedness, film thickness, average refractive index, and birefringence were chosen to match experimental films.

By examining the spectra in Fig. 5, we note that in each case the primary reflection band is stronger than the inverted reflection band, even when the inverted band appears at higher frequencies where the local linear birefringence is increased by dispersion. This may be due to the physical structure of a polygonal helix. Unlike in a CLC, the relative arrangement of the form-birefringent ellipsoids in a given plane of a polygonal helix is related to the ellipsoids in another plane because they are constituents of distinct helical columns. The fixed arrangement of ellipsoids allows a polygonal helix to be assigned a unique physical handedness, which strengthens the primary reflection band because the handedness of the physical microstructure and the optical response are equal. This may also explain why the primary reflection band of a square spiral is not completely negated by the overlapping inverted reflection band. Simulations that decompose a chiral GLAD film into a stack of biaxial plates result in fairly straightforward and accurate models, however, they do not account for the microscopic ordering of the form-birefringent ellipsoids. In the future, more sophisticated numerical simulations may be needed to fully appreciate the influence of a film's microstructure on its optical properties.

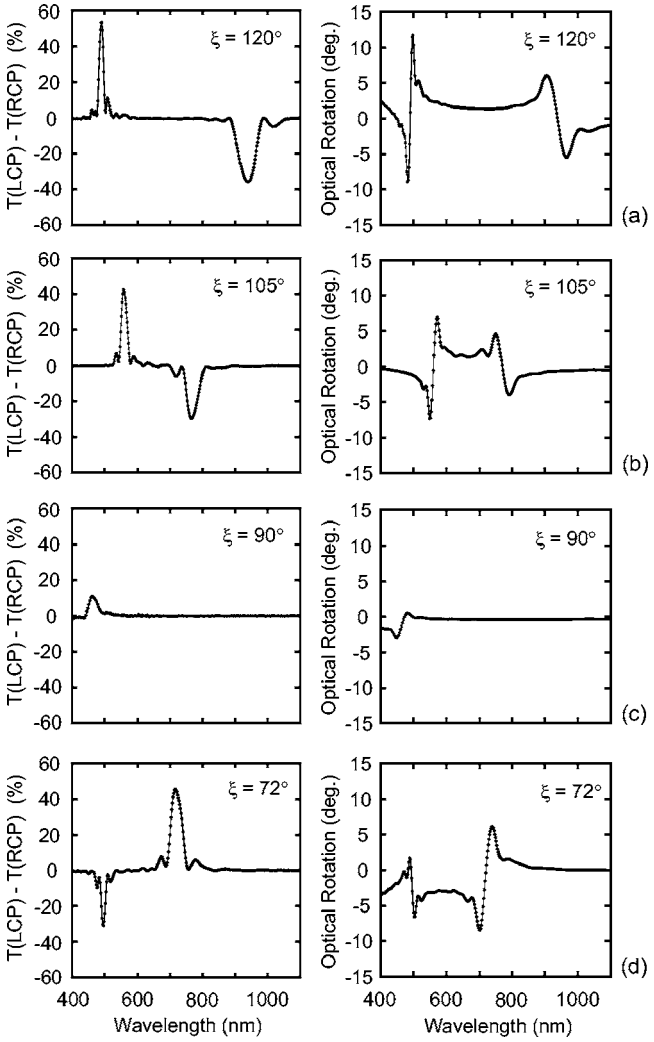

FIG. 5. Selective transmittance of circularly polarized light and optical rotation of linearly polarized light in right-handed polygonal helix thin films: (a) 18-turn, 245-nm-pitch triangle helix; (b) 14-turn, 285-nm-pitch star helix; (c) 7-turn, 240-nm-pitch square helix; and (d) 10-turn, 375-nm-pitch pentagon helix.

VI. DEFECT MODES IN POLYGONAL HELICES

The incorporation of a twist defect was used to create a passband within the circular reflection bands of a triangle polygonal helix. The twist defect was created by abruptly rotating the substrate 90° exactly halfway through the deposition, placing the defect at the center of the helical thin-film structure. A 90°-twist defect creates a π phase shift, placing the spectral hole at the center of each circular reflection band. The resultant selective transmittance spectrum is shown in Fig. 8. The defect mode is clearly visible in both the primary reflectance band at 529 nm and the inverted band at 1010 nm.

An isotropic spacing layer, placed at the center of a helical film, will also produce a spectral-hole filter. A spacing layer whose optical thickness is equal to one-quarter wavelength can generate the same π phase shift that is created by a 90°-twist defect. The only difference is that the phase shift created by a spacing layer is wavelength dependent whereas the phase shift caused by a twist defect is not. To demonstrate this effect, a three-section GLAD film was fabricated,

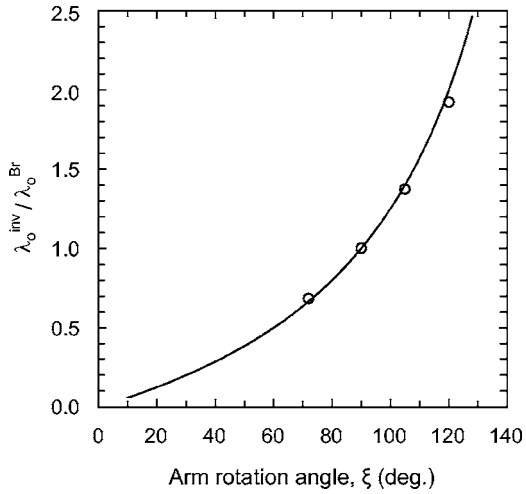

FIG. 6. The wavelength of the inverted reflection band is dependent on the angular rotation between arms of a polygonal helix.

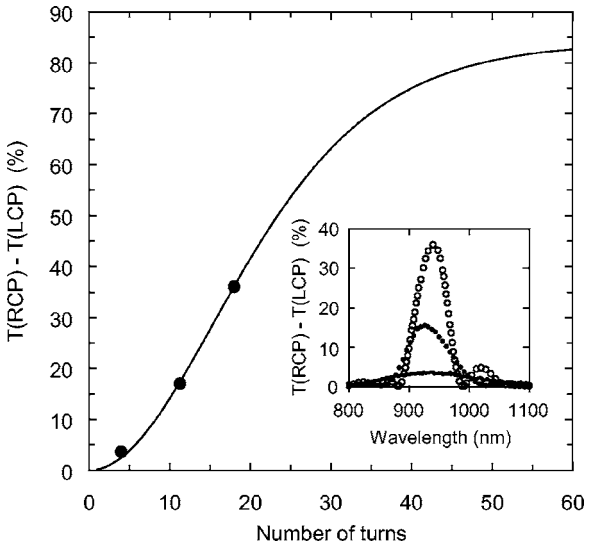

FIG. 7. The selective transmittance of circularly polarized light exhibited by triangle helix is strengthened by adding more turns to the helix. A transfer-matrix method simulation was used to generate the solid line, while the inset shows experimental measurements of the inverted reflection bands taken from a 4-turn, 11.3-turn, and 18-turn helix.

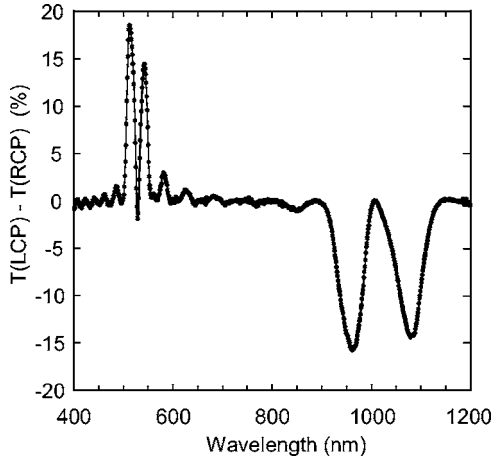

FIG. 8. The selective transmittance of circularly polarized light in a 14-turn triangle helix containing a central 90°-twist defect. The defect mode is present in both the primary and inverted reflection bands.

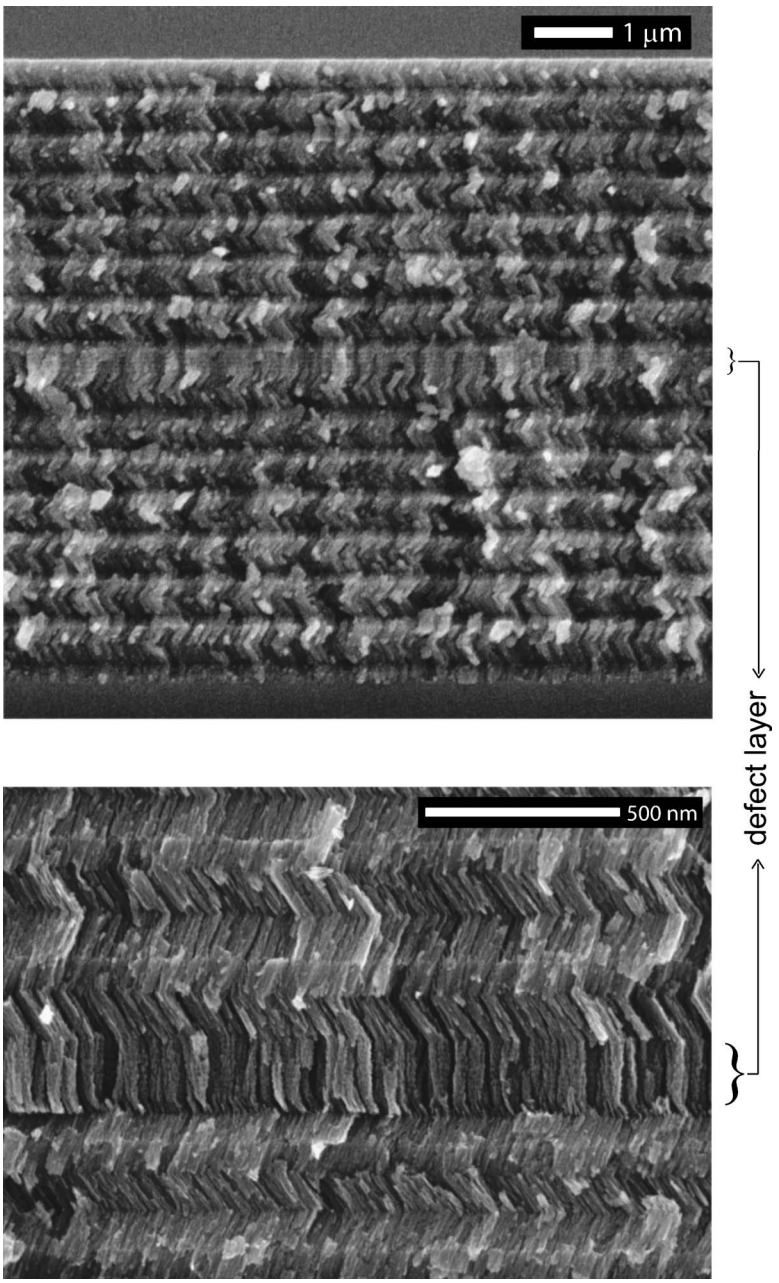

FIG. 9. A side view of a 14-turn triangle helix, containing a central spacing-layer defect and a close-up view of the defect, which is created by a 150-nm-thick layer of uniaxial vertical posts.

consisting of a layer of vertical posts sandwiched between two identical polygonal helices. The helical sections of the film consist of a 7-turn triangle helix with a right-handed structure and 275 nm pitch. The vertical posts were generated by rapid substrate rotation, creating a uniaxial structure which is isotropic in the plane of the substrate. The spacing layer thickness was grown to 150 nm, approximately equal to one-half of the physical pitch of the helix, creating a 2π phase shift at λ_o^{Br}, leaving the primary circular reflection band unaffected. However, at λ_o^{inv} the spacing layer generates a π phase shift since $\lambda_o^{\mathrm{inv}}=2\lambda_o^{\mathrm{Br}}$ for a triangle helix. SEM images highlighting the physical structure and morphology of the spacing layer are shown in Fig. 9, and the selective transmittance spectrum is shown in Fig. 10. Only the inverted reflection band contains the spectral hole, shown at 1030 nm, while the primary reflection band is left intact.

Variable angle spectroscopic ellipsometry was used to measure shift in the spectral hole with changes to the angle of incidence (AOI). The twist-defect triangle helix discussed in reference to Fig. 8 was measured. The frequency shift of the reflectance spectrum is shown in Fig. 11, and the change in the center wavelength of the bandpass is plotted versus $\cos^2\theta$ in the inset. The position of the defect state can be finely tuned to shorter wavelengths by simply tilting the filter.

VII. CONCLUSION

The optical characteristics of polygonal helices are unique to chiral filters. We have shown how GLAD can be used to create a polygonal helix, which is composed of discrete biaxial layers that make abrupt rotations about the substrate normal. While the helical thin-film structure can be assigned a definite physical handedness, the optical properties exhibit a dual-handed response. At the Bragg wavelength, a polygonal helix reflects circularly polarized light

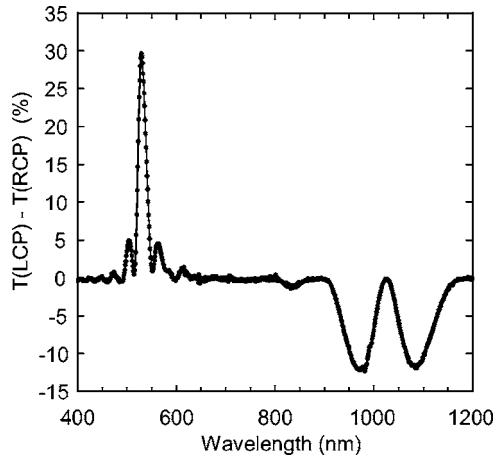

FIG. 10. The selective transmittance of circularly polarized light in a 14-turn triangle helix containing a spacing layer defect. The defect mode only appears in the inverted reflection band at 1030 nm because its optical thickness is equal to one half-wave at the Bragg wavelength, leaving the primary reflection band unaltered.

whose handedness is the same as that of the helical structure. At a second wavelength, the same polygonal helix reflects circularly polarized light of opposite handedness. The wavelength dependence of this inverted reflection band was shifted simply by changing the rotation angle between arms of a polygonal helix during film fabrication. We also used a twist defect and a spacing layer defect to introduce a bandpass within the circular reflection bands of a triangle-type polygonal helix. A twist-defect produces a constant phase discontinuity, which places the spectral hole within both reflection bands of a polygonal helix. A spacing layer defect creates a phase shift that is wavelength dependent, which can be used to create a narrow bandpass that appears within one circular reflectance band of a polygonal helix and not the other. There are several advantages of using a polygonal helix to produce chiral thin-film filters. Optical monitoring of the deposition rate during thin-film fabrication is more accurate than a crystal oscillator and easier to implement for a polygonal helix film than a conventional helix. A polygonal helix also allows for greater structural anisotropies. In a regular helix, the continuous substrate rotation during film deposition inhibits the fanning of the columnar microstructure. Conversely, the lack of substrate motion during the growth of each arm of a polygonal helix allows the tilted columns to freely fan out in directions perpendicular to the deposition plane. Future work will focus on further experimental measurements of polygonal helices while attempting to incorporate these chiral filters into functional devices.

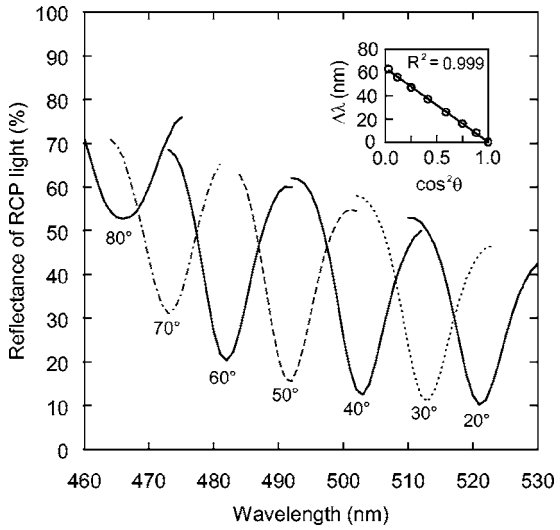

FIG. 11. The frequency of a spectral-hole can be shifted by simply tilting the filter. From 0° AOI to 80° AOI, the narrow bandpass shifts 63 nm.

ACKNOWLEDGMENTS

The authors would like to thank the generous financial support provided by the Natural Sciences and Engineering Research Council of Canada, the Alberta Informatics Circle of Research Excellence, the Alberta Heritage Scholarship Fund, and Micralyne Inc. The authors would also like to recognize the excellent SEM imaging provided by Daniel Salamon from the Canadian National Institute of Nanotechnology and George D. Braybrook from the University of Alberta.

[1] E. Yablonovitch, Phys. Rev. Lett. **58**, 2059 (1987).
[2] S. John, Phys. Rev. Lett. **58**, 2486 (1987).
[3] M. Bayindir, E. Ozbay, E. Temelkuran, M. M. Sigalas, C. M. Soukoulis, R. Biswas, and K. M. Ho, Phys. Rev. B **63**, 081107 (2001).
[4] M. O. Jensen and M. J. Brett, Opt. Express **13**, 3348 (2005).
[5] D. J. Broer, J. Lub, and G. N. Mol, Nature (London) **378**, 467 (1995).
[6] D. M. Shin, D. M. Song, and Y. B. Kim, Mol. Cryst. Liq. Cryst. **425**, 431 (2004).
[7] A. Lakhtakia and V. C. Venugopal, Microwave Opt. Technol. Lett. **17**, 135 (1998).
[8] A. Lakhtakia, M. W. McCall, J. A. Sherwin, Q. H. Wu, and I. J. Hodgkinson, Opt. Commun. **194**, 33 (2001).
[9] P. G. de Gennes, *The Physics of Liquid Crystals*, 2nd ed. (Clarendon, Oxford, 1993).
[10] K. Robbie and M. Brett, J. Vac. Sci. Technol. A **15**, 1460 (1997).
[11] K. Robbie, J. Sit, and M. Brett, J. Vac. Sci. Technol. B **16**, 1115 (1998).
[12] I. Hodgkinson and Q. H. Wu, Appl. Opt. **38**, 3621 (1999).
[13] I. J. Hodgkinson, Q. H. Wu, and L. De Silva, Proc. SPIE **4806**, 118 (2002).
[14] I. J. Hodgkinson, A. Lakhtakia, Q. H. Wu, L. De Silva, and M. W. McCall, Opt. Commun. **239**, 353 (2004).
[15] A. Lakhtakia, V. C. Venugopal, and M. W. McCall, Opt. Commun. **177**, 57 (2000).
[16] I. J. Hodgkinson, Q. H. Wu, K. E. Thorn, A. Lakhtakia, and M. W. McCall, Opt. Commun. **184**, 57 (2000).
[17] O. Painter, R. K. Lee, A. Scherer, A. Yariv, J. D. O'Brien, P. D. Dapkus, and I. Kim, Science **284**, 1819 (1999).
[18] T. Hattori, N. Tsurumachi, and H. Nakatsuka, J. Opt. Soc. Am. B **14**, 348 (1997).
[19] J. S. Foresi *et al.*, Nature (London) **390**, 143 (1997).
[20] J. Schmidtke, W. Stille, and H. Finkelmann, Phys. Rev. Lett. **90**, 083902 (2003).
[21] M. Ozaki, R. Ozaki, T. Matsui, and K. Yoshino, Jpn. J. Appl. Phys., Part 2 **42**, L472 (2003).
[22] D. Vick, T. Smy, and M. J. Brett, J. Mater. Res. **17**, 2904 (2002).
[23] K. J. Robbie and M. J. Brett, U.S. Patent No. 5,866,204 (February 2, 1999); K. J. Robbie and M. J. Brett, U.S. Patent No. 6,206,065 (March 27, 2001); K. J. Robbie and M. J. Brett, U.S. Patent No. 6,248,422 (June 19, 2001).
[24] J. C. Sit, D. Vick, K. Robbie, and M. J. Brett, J. Mater. Res. **14**, 1197 (1999).
[25] D. Vick, Y. Y. Tsui, M. J. Brett, and R. Fedosejevs, Thin Solid Films **350**, 49 (1999).
[26] M. J. Colgan and M. J. Brett, Thin Solid Films **389**, 1 (2001).
[27] J. N. Broughton and M. J. Brett, Electrochim. Acta **49**, 4439 (2004).
[28] G. K. Kiema and M. J. Brett, J. Electrochem. Soc. **151**, E194 (2004).
[29] S. R. Kennedy and M. J. Brett, Appl. Opt. **42**, 4573 (2003).

[30]K. D. Harris, D. Vick, E. J. Gonzalez, T. Smy, K. Robbie, and M. J. Brett, Surf. Coat. Technol. **138**, 185 (2001).
[31]G. K. Kiema, M. J. Colgan, and M. J. Brett, Sol. Energy Mater. Sol. Cells **85**, 321 (2005).
[32]S. R. Kennedy and M. J. Brett, J. Vac. Sci. Technol. B **22**, 1184 (2004).
[33]J. B. Sorge, A. C. van Popta, J. C. Sit, and M. J. Brett, Mater. Res. Soc. Symp. Proc. **846**, DD10.17 (2004).
[34]D. E. Aspnes, Thin Solid Films **89**, 249 (1982).
[35]I. Hodgkinson, Q. H. Wu, and S. Collett, Appl. Opt. **40**, 452 (2001).
[36]A. C. van Popta, J. C. Sit, and M. J. Brett, Appl. Opt. **43**, 3632 (2004).
[37]K. N. Rao, Opt. Eng. **41**, 2357 (2002).
[38]A. C. van Popta, J. C. Sit, and M. J. Brett, Proc. SPIE **5464**, 198 (2004).
[39]S. Tsoi, E. Fok, J. C. Sit, and J. G. C. Veinot, Langmuir **20**, 10771 (2004).
[40]E. Collett, *Polarized Light: Fundamentals and Applications* (Marcel Dekker, New York, 1993).
[41]I. J. Hodgkinson, Q. H. Wu, M. Arnold, M. W. McCall, and A. Lakhtakia, Opt. Commun. **210**, 201 (2002).
[42]I. J. Hodgkinson and Q. H. Wu, *Birefringent Thin Films and Polarizing Elements* (World Scientific, Singapore, 1997).
[43]P. D. Sunal, A. Lakhtakia, and R. Messier, Opt. Commun. **158**, 119 (1998).
[44]A. Lakhtakia and R. Messier, *Sculptured Thin Films: Nanoengineered Morphology and Optics* (SPIE, Bellingham, WA, 2005).